ACS APPLIED NANO MATERIALS

www.acsanm.org Letter

Enhanced Broadband and Harmonic Upconversion from Coupled Semiconductor and Metal Nanoparticle Films

Nathan J. Spear, Kent A. Hallman, Emil A. Hernández-Pagán, Roderick B. Davidson II, Summer L. Arrowood, Amanda L. Wistuba, Wenze Tan, Richard F. Haglund, and Janet E. Macdonald*

Cite This: *ACS Appl. Nano Mater.* 2020, 3, 3144–3150 Read Online

ACCESS | Metrics & More | Article Recommendations | Supporting Information

ABSTRACT: The enhancement of the nonlinear optical properties of hybrid nanoparticle films by coupling between metallic and plasmonic semiconducting nanoparticles is shown. A heterostructure comprising CuS and Au nanoparticle films separated by a thin layer of insulating ligands enhanced the yield of second-harmonic light by a factor of 3.3 compared with the sum of the constituent nanoparticles on their own. Heterostructures were fabricated with scalable solution-processing techniques that can create devices of arbitrary geometry. In addition to harmonic generation, the multiple-photon photoluminescence response of Au, CuS, and heterostructured films is also explored.

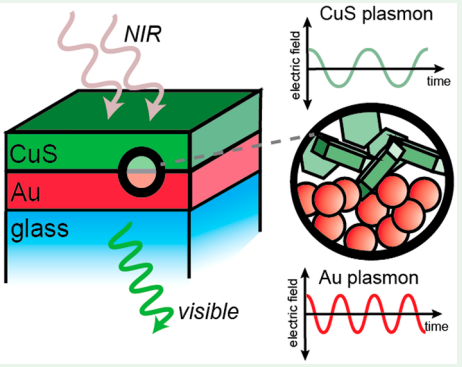

KEYWORDS: *heterostructure, second-harmonic generation, multiphoton photoluminescence, plasmon, nonlinear optical material, gold nanoparticle, copper sulfide nanoparticle*

The second-order nonlinear response of metal nanostructures is a well-known example of the effects of both the broken spatial symmetry at surfaces and the resonance enhancement generated through localized surface plasmon resonances (LSPRs). Plasmonic resonances of coupled metal nanostructures can enhance the nonlinear properties of materials through near-field dipole−dipole coupling[1,2] and also amplify the nonlinear response of metallic materials themselves.[3,4] In the specific case of second-harmonic generation (SHG), further enhancements can be achieved by designing nanostructures with additional resonances at the fundamental, second harmonic, or both. Examples include arrays of split ring resonators,[5] gold nanofeatures that support Fano resonances,[6] and LSPR active gold nanoparticles that couple into optical whispering gallery modes.[7] The enhancement of SHG via the coupling of two plasmons has also been demonstrated using arrays of differently sized or shaped plasmonic features in specific geometric arrangements[8−11] or by combining metals with differing plasmon energies (e.g., biplasmonic heterobimetallic Au/Ag nanorods[12]).

The complexity of the structures for the multiplasmonic enhancement of SHG has driven a near-total reliance on lithography to obtain precise control over the composition, shape, and arrangement of the individual nanostructures. However, lithography imposes significant limitations on the device geometry and scalability. Alternatively, colloidal nanoparticles can provide similar control over the composition and shape of the nanostructures and yet are also amenable to solution processing and conformal deposition.

The synthesis of metal nanoparticles with prominent LSPR absorption of varying compositions and shapes, typically of Au, Ag, and their alloys, is a maturing field. The narrow-band LSPRs of these nanomaterials are tunable from the UV through the visible and near-infrared (NIR)[13] and have been widely employed for plasmon-enhanced SHG. However, plasmon resonances in metal nanoparticles tend to be relatively spectrally narrow, and thus this strategy for designer coupled plasmonic SHG structures tends to be useful primarily for a single input/output frequency pair.

Heterostructures that couple the plasmon of a metal with the exciton of a semiconductor have been shown to enhance the generation of second-harmonic light.[1,14,15] In this case, SHG from the semiconductor nanocrystal is enhanced by the local-field effects of the metal plasmon resonance.[16] These studies showed that the separation of the semiconductor and the metal components was important because direct contact

Received: January 8, 2020
Accepted: April 3, 2020
Published: April 3, 2020

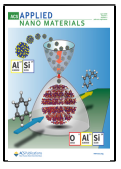

https://dx.doi.org/10.1021/acsanm.0c00064
ACS Appl. Nano Mater. 2020, 3, 3144–3150

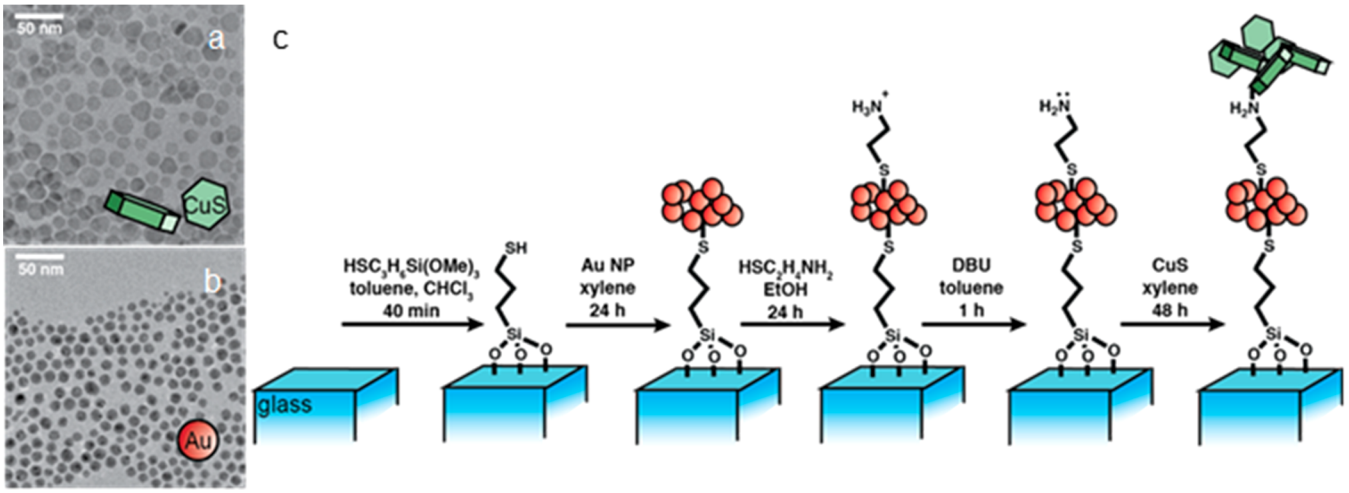

Figure 1. (a) TEM and schematics of CuS nanoparticles. (b) TEM and schematic of Au nanoparticles. (c) Schematic of the film deposition process.

between them allows an interfacial charge transfer that damps the SHG.[17]

Many semiconductors, including the large family of copper chalcogenides, have NIR plasmon resonances that can be tuned by changing composition, doping, or morphology.[18] These materials have untapped potential in plasmon−plasmon coupled heterostructured nanomaterials for SHG. Moreover, these semiconductor plasmon resonances turn out to be relatively broad.[19] Therefore, a large spectral bandwidth can be covered through many potential combinations of semiconductor nanocrystals with an LSPR at a fundamental frequency, which couple resonantly to a metal nanoparticle with an LSPR at the second-harmonic frequency. These combinations of resonantly coupled plasmonic nanocrystals are a promising strategy for the broadly tunable emission of upconverted light, with the added benefit that the nanoparticle constituents are synthesizable by standard solvothermal techniques and are solution-processable into films.

Here we demonstrate for first time that plasmonic semiconductors can be used in conjunction with metallic nanoparticles to enhance SHG or other multiphoton upconversion mechanisms. We specifically study a heterostructure comprising a bilayer of nanoparticle films. The first contains CuS (covellite) nanoparticles that feature a broad LSPR in the NIR ($\lambda_{LSPR,CuS}$ = 900−1600) nm, and the second layer contains gold nanoparticles that feature a visible spectrum LSPR ($\lambda_{LSPR,Au}$ = 510−610 nm) when excited by a femtosecond Nd:glass laser (1050 nm).

Covellite exhibits electronic properties typical of a heavily doped semiconductor due to an intrinsically high concentration of holes (h^+). These holes act as positive charge carriers, giving covellite a p-type character and a plasmon resonance that absorbs strongly from 900 to 1600 nm.[20] Plasmonic states in covellite function as intermediate virtual states in two-photon absorption and in coupled plasmon−exciton complexes for two-photon photoluminescence. In CuS, the second harmonic of the bluest edge of the plasmon resonance overlaps with the onset of excitonic absorption (2.5 eV, 496 nm, just below the conduction-band edge). A threefold enhancement of two-photon photoluminescence in covellite was demonstrated at an excitation wavelength of 855 nm, where this plasmon−exciton energy-matching condition occurs.[21] Excitations at lower photon energies, such as the 1050 nm light used here, are insufficient to produce an excitonic state via two-photon absorption.

However, in the Au/CuS heterostructure, with excitation at 1050 nm, enhanced SHG exceeding the incoherent sum of the individual components was still observed. Upconverted light produced by SHG was separated from that produced by multiphoton photoluminescence (MPPL) by using appropriate filters; in addition, the full spectrum of upconverted light was also measured. Both the MPPL and SHG signals were enhanced by the heterostructure; at high pump laser intensities, the enhancement of the MPPL was small compared with the SHG. The discovery and exploitation of this SHG enhancement with colloidal nanocrystals could lead to the development of efficient nonlinear materials on planar or nonplanar surfaces through solution processing and, with the further development of the colloidal chemistry, of nonbleaching, nonblinking, free-standing, upconversion nanocrystal hybrid systems as biological imaging probes and contrast agents.

Au and CuS nanoparticles were synthesized using standard solvothermal techniques (Figure 1a,b). The nanoparticles were then assembled into heterostructured films using a facile bath method,[22,23] as diagrammed in Figure 1c. Descriptions of Au and CuS nanoparticle syntheses,[20,24] optical characterization methods, and heterostructure characterization are available in Section 4 of the Supporting Information.

Vertical and lateral film inhomogeneities in CuS deposition, shown by profilometry and SEM imaging of the hybrid films, produced changes in the nonlinear response, as discussed in Figure S6. Additionally, a laser-induced annealing effect on the film was demonstrated upon repeated exposure of the sample to the laser. Initial decreases in the signal leveled off after several exposures to the laser, permitting stable measurement conditions, as shown in Figure S5. These two factors were compensated by controlling the placement of the focal spot on the sample and ensuring premeasurement exposure for ∼15 min to the laser.

The anisotropic geometry of CuS nanoparticles allows the excitation of both transverse and longitudinal plasmon modes; however, they exhibit only a single broad, intense extinction band due to the overlap of the two allowed modes.[20] For Au nanoparticles, the isotropic shape facilitates the dominance of a single plasmon resonance centered at 560 nm (Figure 2a). The

https://dx.doi.org/10.1021/acsanm.0c00064
ACS Appl. Nano Mater. 2020, 3, 3144−3150

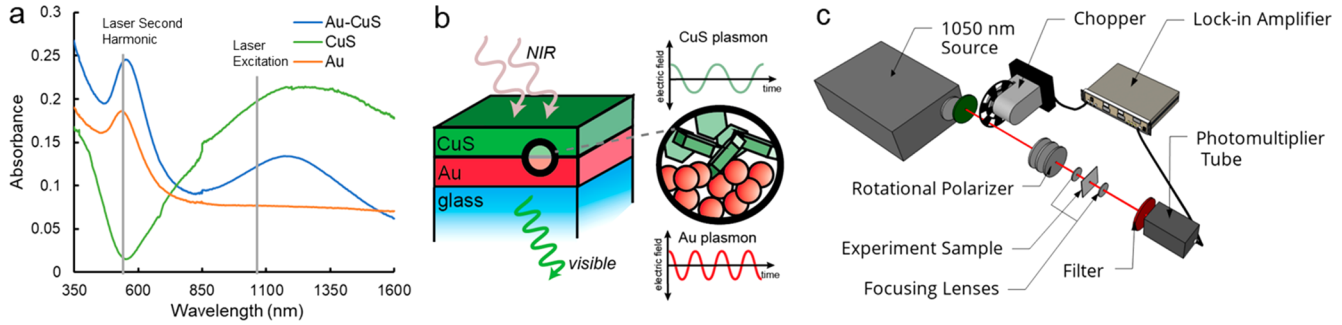

Figure 2. (a) UV−vis−NIR spectrophotometry of typical nanoparticle films deposited on glass microscope slides. The fundamental wavelength of the pump laser and the second harmonic are denoted by gray lines. (b) Illustration of SHG enhancement by plasmonic resonance in Au/CuS hybrid film. (c) Experimental configuration for measuring nonlinear optical properties.

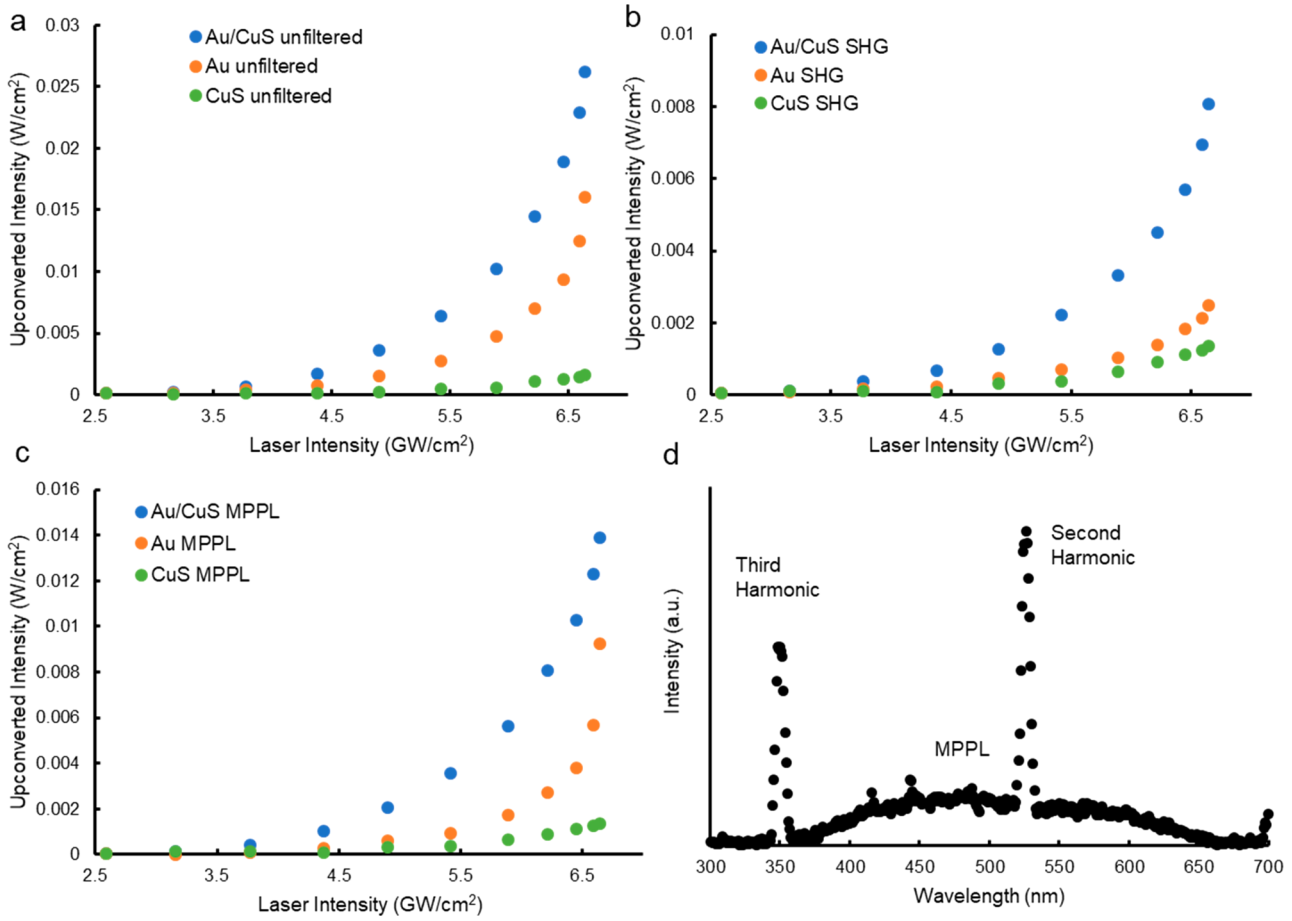

Figure 3. (a) Intensity of the unfiltered visible light generated versus the input laser intensity for each film type: Au only (orange), CuS only (green), and heterostructure (blue). (b) Intensity of light generated by the films at the second harmonic of the pump laser. (c) Intensity of visible light produced by the films not at the second harmonic. This light corresponds to upconversion by MPPL. (d) Spectrum of output light produced by the nanoparticle heterostructure demonstrating upconversion by both harmonic generation and multiple-photon photoluminescence mechanisms.

presence of Au nanoparticles on the functionalized glass slide was confirmed by both the Au plasmon resonance peak ($\lambda_{LSPR,Au}$ = 560 nm) in UV−vis−NIR spectroscopy, as shown in Figure 2a, and SEM micrographs (Figure S2), which show an even coverage of Au nanoparticles on the glass surface. Profilometry indicated that the film was multilayered, as the ~30 nm thickness of a film layer is greater than the diameter of the Au nanoparticles (~7 nm) (Figure S2). Profilometry also demonstrated that CuS films were approximately twice as thick as than those of Au. This ensured a sufficient upconverted signal from films containing only CuS nanoparticles, despite their relatively low nonlinear activity.

The deposition of CuS onto the sample was confirmed by the broad CuS plasmon extinction peak ($\lambda_{LSPR,CuS}$ = 1300 nm) in UV−vis−NIR spectroscopy. A comparison of the plasmon extinction between films containing only Au or CuS nanoparticles and nanoparticle heterostructures shows that there is no shift in the linear plasmonic response of either Au or CuS (Figure 2a). Thus an enhancement of nonlinear activity due to shifts in the dielectric environment[25] is unlikely. The shift in

https://dx.doi.org/10.1021/acsanm.0c00064
ACS Appl. Nano Mater. 2020, 3, 3144−3150

plasmon resonance of Au and CuS nanoparticles from solution to film is shown in Figure S3. The nanoparticle films were exposed to 150 fs pulses of radiation from a mode-locked Nd:glass laser operating at 1050 nm wavelength at a pulse repetition frequency of 100 MHz to induce the generation of visible upconverted light, as illustrated in Figure 2c. The beam was attenuated with crossed polarizing filters, and the intensity of the visible light was monitored with a photomultiplier tube (PMT). The PMT was not sensitive in the IR region.

A short-pass optical filter (edge at 720 nm), together with the sensitivity drop of the PMT in that spectral region, reduced the NIR signal from the laser fundamental below the detectable limit. The spectroscopy of an SHG material (BBO), as shown in Figure S4, supports this conclusion by demonstrating the complete attenuation of the fundamental beam and the presence of a peak at 525 nm. All nanoparticle films—CuS, Au, and the hybrid Au/CuS—demonstrated a supralinear intensity response. In addition to SHG at double the frequency of the pump laser fundamental, the LSPR of gold nanostructures, in particular, gold nanorods and dimers, enhances a broad photoluminescence spectrum due to multiple-photon absorption.[26] Multiple-photon photoluminescence (MPPL) has been identified as requiring two-, four-, and six-photon[7] absorptions, although few experiments have been able to separate the influence of two-photon SHG from the MPPL components.[27] In contrast to the sharp SHG signal (set by the bandwidth of the laser), the MPPL feature is a broad emission feature ranging from ∼400−650 nm.[7] Short-pass and notch filters were used to capture the SHG signal and the MPPL, respectively.

Films containing only gold nanoparticles produced a strong nonlinear response consistent with many literature reports (Figure 3a). SHG has been demonstrated in gold nanoparticle arrays, hemispherical gold caps on silica nanospheres, gold dimer nanoantennas, and gold nanorods.[4,28] However, for the Au nanoparticle films, filtering of the upconverted light to capture an SHG or MPPL signal demonstrated that only a small contribution of the upconverted light was from the second harmonic (Figure 3b); instead, most of the output was from the MPPL contribution (Figure 3c). This is likely because SHG from the interior of the gold nanoparticles is unlikely due to their inversion symmetry.

The nonlinear response of the CuS-only films was modest, roughly a factor of 15 less than that of the gold films at the strongest laser intensity employed. This is consistent with their centrosymmetric structure, which prevents SHG from the bulk but allows weak surface SHG enhanced by its NIR plasmon resonance. Additionally, at 1050 nm laser excitation, two-photon absorption is not sufficient to excite valence band electrons of CuS into the conduction band. Thus two-photon absorption followed by second-harmonic emission can only proceed via surface or trap states in the band gap.[29] Correspondingly, the MPPL contribution from films containing only CuS (Figure 3c) was much smaller than the SHG contribution (Figure 3b).

At pump intensities above ∼4 GW/cm^2, the heterostructure films produced a strong nonlinear response. Importantly, the emission from the hybrid films was still greater than the incoherent sum of the two components. To quantify the enhancement due to coupling between the nanoparticles, the visible-light contribution of the nanoparticle components was measured as a fraction of the upconverted light produced by the hybrid films.

$$\chi_j = \frac{I_{\text{hybrid},j}}{(I_{\text{Au},j} + I_{\text{CuS},j})}, \quad j = \text{SHG, MPPL, unfiltered} \tag{1}$$

Thus higher values of χ_j correspond to larger SHG enhancement due to hybridization because less of the hybrid film output is attributable to its nanoparticle components.

Figure 4c plots the values of χ_j for the SHG and MPPL components across the pump laser range of 3.5−7 GW/cm^2. The SHG and MPPL signals are similarly enhanced at lower pump intensities, such that the values of χ_{SHG} and χ_{MPPL} are similar. However, at intensities above 6 GW/cm^2, the high-order dependence of MPPL from the Au nanoparticles reflects the increase in upconverted signal directly attributable to the Au nanoparticles; this, in turn, drives a decrease in χ_{MPPL}. The SHG signal does not exhibit a similar change in the order of response as the MPPL signal, and thus the magnitude of χ_{SHG} remains constant across the full range of laser intensities.

To further quantify the enhancement that film hybridization provides, a modification of the analytical enhancement factor (AEF) defined by Jais et al. was used.[14]

$$\text{AEF} = \frac{I_{\text{Au-CuS}}/\rho_{\text{Au-CuS}}}{I_{\text{Au}}/\rho_{\text{Au}}} \tag{2}$$

where I is the SHG intensity and ρ is the optical density of Au nanoparticles at 525 nm. The enhancement effect strengthens as the input intensity increases for the SHG signal. At the maximum pump laser intensity (6.64 GW/cm^2), the AEF for the SHG signal was 3.3, whereas the AEF for the MPPL signal was 1.7. The measured visible-light intensity as a function of the pump laser intensity was used to construct a double-logarithmic plot of the data whose slope yields the order of the nonlinearity that produces up-conversion.

The values for the slope (b) and intercept (a) of the log−log linear fits for the MPPL-filtered and SHG-filtered data are shown in Tables 1 and 2, respectively. The variances in the fit coefficients are the ±1 standard deviation limits.

An inspection of the log−log plots for the Au films suggests that at the highest pump laser intensities, the order of the nonlinearity actually increases. This is indicated by the increasing slope of the orange line in Figure 4a,b, in the fit to those data above 6 GW/cm^2 (Au high). Although the Au slope increase occurs in both the MPPL and SHG regimes, it is far more prominent in the MPPL regime. This suggests that any observed increase in the order of nonlinearity in the 515−560 nm spectrum is due to the contribution from MPPL overlapping with the SHG signal. This also explains why the order in the SHG regime is greater than two, as would be expected from an SHG signal.

Spectral overlapping of the MPPL and SHG signals caused the response in that part of the spectrum to take on the response characteristics ($n > 2$) of MPPL. This conclusion is supported by the spectrum of the upconverted output (Figure 3d), which convolutes the SHG and MPPL peaks across the 520−540 nm spectrum.

The mechanism of the enhancement awaits further investigation, in particular, using time-resolved techniques to elucidate the dynamics of the harmonics and the broadband MPPL emission. However, we can draw some conclusions. The MPPL mechanism is effective, especially in gold, as a result of intraband transitions in the sp band that occur concurrently with interband d-to-sp transitions to create a d-band hole that serves as the final state for an sp-to-d interband

https://dx.doi.org/10.1021/acsanm.0c00064
ACS Appl. Nano Mater. 2020, 3, 3144−3150

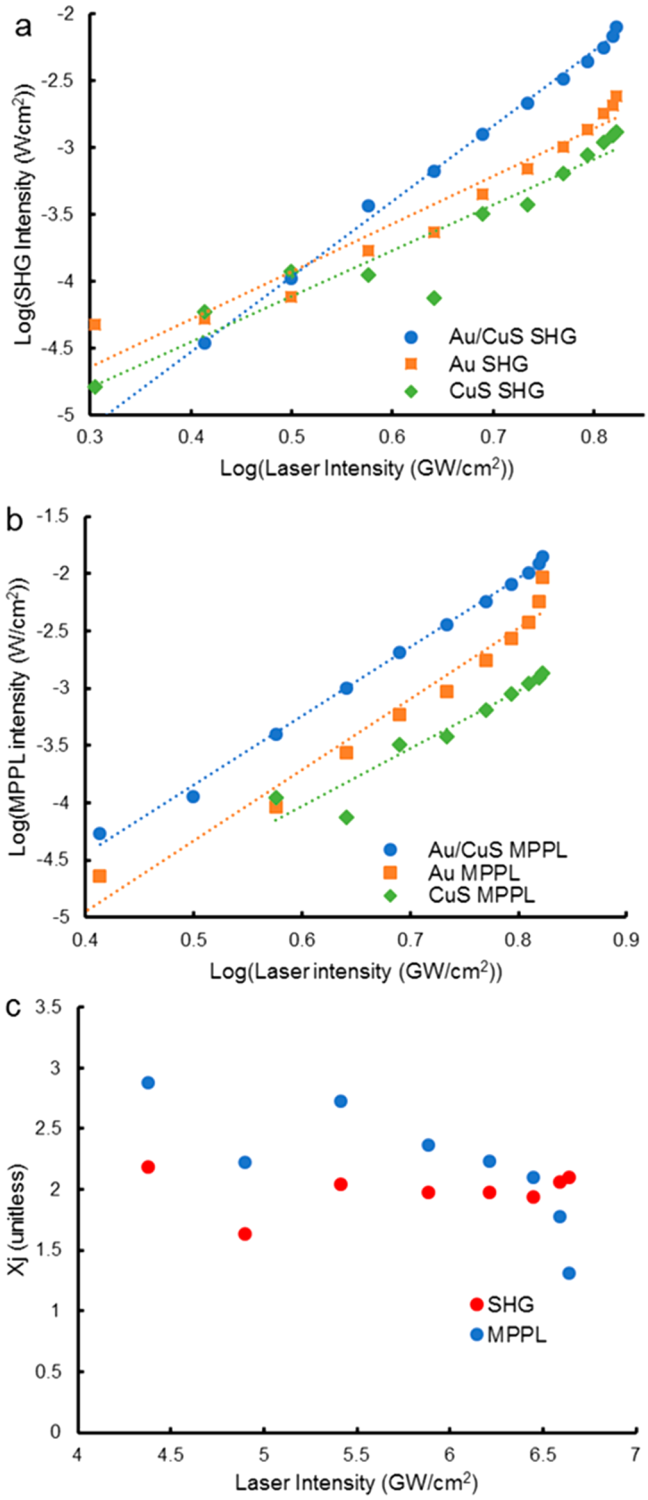

Figure 4. Double-logarithmic plots of the up-converted light intensity as a function of pump laser intensity. (a) Fit for the SHG signal (515−560 nm). (b) Fit for the MPPL signal (560−720 nm). (c) Fraction of upconverted signal in hybrid samples that is directly attributable to the nanoparticle constituents (χ_j, eq 1) for the SHG and MPPL components as a function of pump laser intensity.

transition.[26] The SHG and third-harmonic generation (THG) signals, on the contrary, arise from virtual transitions originating in the d band in gold, where they are quite efficient; a similar mechanism must be operative in the CuS but, to judge from the relative yields in Figure 3a−c, must be much less efficient, even though the hole-rich valence band in CuS might seem to enable virtual multiphoton or multiple-photon transitions.

The enhancement mechanism may be modeled by thinking of the planar components of the heterostructure as resonant, coupled cavities in close but not intimate contact, with the CuS nanodisks resonant near the fundamental frequency of the laser and the gold nanoparticles at the second harmonic. The coupling is weak, with a coupling constant on the order of 10^{-12} if it scales with the relative upconversion intensities in Figure 3b,c. Moreover, this is evidently not the entire story because the largest broadband MPPL signal arises from the heterostructure; this is not explainable either by the combination of intraband and interband transitions seen in gold or by excitonic transitions, which cannot be accessed at these pump photon energies. In particular, the broadband MPPL signal does not extend into the ultraviolet where the THG signal is observed. However, our observations might be consistent with a Förster resonance energy transfer mechanism.

It is interesting to compare the efficiency of SHG from the hybrid nanoparticle films to that of SHG from β-barium borate (BBO), perhaps the most widely used nonlinear harmonic-generating crystal. For laser intensities below the SHG enhancement threshold (4 GW/cm^2), normalized to the thickness of the sample and laser power squared, the BBO and hybrid nanoparticle films have nearly equivalent (2.2::1 Au/CuS:BBO) SHG per unit thickness. On the contrary, at the highest measured pump intensity (6.64 GW/cm^2), when the intensity of the SHG is normalized to sample thickness and the square of the pump laser intensity, the hybrid nanoparticle film has almost an order of magnitude greater yield per unit thickness than BBO (9.2::1). This is about twice the volume-normalized yield from lithographically fabricated gold Archimedean nanospirals.[30] The second-harmonic yield is also proportional to the effective second-order susceptibility, d_{eff}, this implies that the hybrid bilayer has $d_{\text{eff}} \approx 13$ pm/V.

Nanoparticle films containing only Au and CuS nanoparticles were also evaluated. For films with the same optical density of nanoparticles as the hybrid sample, normalized by length and laser power squared, the Au nanoparticle films produced modestly more second-harmonic light than BBO (2.8::1), and the CuS nanoparticle films produced less visible light than BBO (0.2::1). This further highlights the relatively low nonlinear response of CuS nanoparticles when stimulated at 1050 nm without the presence of the Au nanoparticles. Optimization of the films and nanocrystal placement is expected to further improve this material property.

CONCLUSIONS

In summary, Au nanospheres have a plasmon resonance near the second harmonic of the fundamental plasmonic resonance of CuS nanoparticles. Hybrid CuS/Au nanoparticle heterostructures exhibited an analytic enhancement factor for the second-harmonic signal of 3.3, exhibiting greater second-harmonic yield than the sum of either nanoparticle film alone. This suggests that there is a coupling effect between the CuS nanoparticles and the Au nanoparticles. The presence of Au nanoparticles attenuates the bleach of the CuS nonlinear absorption in hybrid films. The hybrid films exhibit greater upconversion efficiency per unit thickness than BBO, a high-performance nonlinear crystal.

https://dx.doi.org/10.1021/acsanm.0c00064
ACS Appl. Nano Mater. 2020, 3, 3144−3150

Table 1. Values of log−log Fitting Coefficients for MPPL-Filtered Data (400−502, 562−700 nm)

	Au film (low)	Au film (high)	Au/CuS	CuS film
a	−7.42 ± 0.31	−12.3 ± 2.0	−6.84 ± 0.078	−7.05 ± 0.44
b	6.17 ± 0.44	12.3 ± 2.5	5.99 ± 0.11	5.03 ± 0.59
R^2	0.96	0.89	0.99	0.91

Table 2. Values of log−log Fitting Coefficients for SHG-Filtered Data (522−552 nm)

	Au film	Au/CuS	CuS film
a	−5.72 ± 0.18	−6.79 ± 0.051	−5.82 ± 0.23
b	3.57 ± 0.27	5.65 ± 0.075	3.43 ± 0.34
R^2	0.95	0.99	0.91

This work demonstrates that a thin-film heterostructure that places semiconducting and metallic nanoparticles in close proximity can enhance nonlinear optical properties by coupling of plasmonic excitations. Such a material system has important advantages for nonlinear optical materials, in that plasmonic processes are ultrafast compared with excitonic processes and due to the ease with which the nanoparticle films can be fabricated via solution processing. Many plasmonic metal and semiconducting combinations can be envisioned with plasmon bands ranging from the NIR to the UV, making this design highly tunable. In this particular system, the plasmon resonance is at a maximum near the favored wavelength for dispersionless propagation in the telecommunications band. In these nanoparticle films, phase matching is not required. This development in nanocrystal-based nonlinear optical materials will allow the reduced size of optical components, reaching toward the domain of planar nano-optical devices. Further exploration of the dependence of the SHG yield on the interaction distance between coupled plasmonic elements, the effect of coupling between plasmonic elements on the THG, and the effect of alternative material systems will allow an increased understanding of the fundamental mechanisms that govern coupling between plasmonic nanoparticles.

■ ASSOCIATED CONTENT

Supporting Information

The Supporting Information is available free of charge at https://pubs.acs.org/doi/10.1021/acsanm.0c00064.

Section S1. Film Characterization and Performance. Section S2. Calculation of Linear and Nonlinear Absorption Coefficients. Section S3. Model of Pump Light and Estimate of Linear and Nonlinear Absorption Coefficients. Section S4. Experimental Methods (PDF)

■ AUTHOR INFORMATION

Corresponding Author

Janet E. Macdonald − *Department of Chemistry and Vanderbilt Institute of Nanoscale Science and Engineering, Vanderbilt University, Nashville, Tennessee 37235, United States;* orcid.org/0000-0001-6256-0706; Phone: (615) 322-2719; Email: janet.macdonald@vanderbilt.edu; Fax: (615) 343-1234

Authors

Nathan J. Spear − *Department of Chemistry and Vanderbilt Institute of Nanoscale Science and Engineering, Vanderbilt University, Nashville, Tennessee 37235, United States;* orcid.org/0000-0002-0881-6798

Kent A. Hallman − *Vanderbilt Institute of Nanoscale Science and Engineering and Department of Physics and Astronomy, Vanderbilt University, Nashville, Tennessee 37235, United States*

Emil A. Hernández-Pagán − *Department of Chemistry and Vanderbilt Institute of Nanoscale Science and Engineering, Vanderbilt University, Nashville, Tennessee 37235, United States;* orcid.org/0000-0002-3516-8052

Roderick B. Davidson II − *Vanderbilt Institute of Nanoscale Science and Engineering and Department of Physics and Astronomy, Vanderbilt University, Nashville, Tennessee 37235, United States*

Summer L. Arrowood − *Department of Chemistry and Vanderbilt Institute of Nanoscale Science and Engineering, Vanderbilt University, Nashville, Tennessee 37235, United States*

Amanda L. Wistuba − *Department of Physics and Astronomy, Vanderbilt University, Nashville, Tennessee 37235, United States*

Wenze Tan − *Department of Physics and Astronomy, Vanderbilt University, Nashville, Tennessee 37235, United States*

Richard F. Haglund − *Vanderbilt Institute of Nanoscale Science and Engineering and Department of Physics and Astronomy, Vanderbilt University, Nashville, Tennessee 37235, United States*

Complete contact information is available at: https://pubs.acs.org/10.1021/acsanm.0c00064

Notes

The authors declare no competing financial interest.

■ ACKNOWLEDGMENTS

The research and all authors were supported by Vanderbilt's Office of the Provost Interdisciplinary Discovery Grant. S.L.A. thanks the D. Stanley and Ann T. Tarbell Endowment Fund. K.A.H. acknowledges support for building and calibrating the optical train from the National Science Foundation (ECCS1509740). A.L.W. was supported by the National Science Foundation Research Experience for Undergraduates program in the Vanderbilt Department of Physics and Astronomy (PHYS 1852158). R.B.D. was supported during the initial proof-of-concept experiments by the U.S. Department of Energy (DE-FG02-01ER45916). We thank the staff of the Vanderbilt Institute of Nanoscale Science and Engineering for use of the Osiris TEM and Merlin SEM, in particular, Dr. Anthony Hmelo for his advice and guidance and Professor Sharon Weiss for the use of the monochromator.

■ REFERENCES

(1) Grinblat, G.; Rahmani, M.; Cortés, E.; Caldarola, M.; Comedi, D.; Maier, S. A.; Bragas, A. V. High-Efficiency Second Harmonic Generation from a Single Hybrid Zno Nanowire/Au Plasmonic Nano-Oligomer. *Nano Lett.* **2014**, *14* (11), 6660−6665.

(2) Zhang, Y.; Manjavacas, A.; Hogan, N. J.; Zhou, L.; Ayala-Orozco, C.; Dong, L.; Day, J. K.; Nordlander, P.; Halas, N. J. Toward Surface Plasmon-Enhanced Optical Parametric Amplification (SPOPA) with

Engineered Nanoparticles: A Nanoscale Tunable Infrared Source. *Nano Lett.* **2016**, *16* (5), 3373−3378.
(3) Bachelier, G.; Russier-Antoine, I.; Benichou, E.; Jonin, C.; Brevet, P.-F. Multipolar Second-Harmonic Generation in Noble Metal Nanoparticles. *J. Opt. Soc. Am. B* **2008**, *25* (6), 955.
(4) Zhang, Y.; Grady, N. K.; Ayala-Orozco, C.; Halas, N. J. Three-Dimensional Nanostructures as Highly Efficient Generators of Second Harmonic Light. *Nano Lett.* **2011**, *11* (12), 5519−5523.
(5) Niesler, F. B. P.; Feth, N.; Linden, S.; Wegener, M. Second-Harmonic Optical Spectroscopy on Split-Ring-Resonator Arrays. *Opt. Lett.* **2011**, *36* (9), 1533−1535.
(6) Thyagarajan, K.; Butet, J.; Martin, O. J. F. Augmenting Second Harmonic Generation Using Fano Resonances in Plasmonic Systems. *Nano Lett.* **2013**, *13*, 1847.
(7) Ai, Q.; Gui, L.; Paone, D.; Metzger, B.; Mayer, M.; Weber, K.; Fery, A.; Giessen, H. Ultranarrow Second-Harmonic Resonances in Hybrid Plasmon-Fiber Cavities. *Nano Lett.* **2018**, *18* (9), 5576−5582.
(8) Celebrano, M.; Wu, X.; Baselli, M.; Großmann, S.; Biagioni, P.; Locatelli, A.; De Angelis, C.; Cerullo, G.; Osellame, R.; Hecht, B.; et al. Mode Matching in Multiresonant Plasmonic Nanoantennas for Enhanced Second Harmonic Generation. *Nat. Nanotechnol.* **2015**, *10* (5), 412−417.
(9) Czaplicki, R.; Husu, H.; Siikanen, R.; Mäkitalo, J.; Kauranen, M.; Laukkanen, J.; Lehtolahti, J.; Kuittinen, M. Enhancement of Second-Harmonic Generation from Metal Nanoparticles by Passive Elements. *Phys. Rev. Lett.* **2013**, *110* (9), 1−5.
(10) Cheng, Z. Q.; Li, Z. L.; Luo, X.; Shi, H. Q.; Luo, C. L.; Liu, Z. M.; Nan, F. Enhanced Second Harmonic Generation by Double Plasmon Resonances in Mesoscale Flower-like Silver Particles. *Appl. Phys. Lett.* **2019**, *114* (1), 011901.
(11) Yang, K. Y.; Butet, J.; Yan, C.; Bernasconi, G. D.; Martin, O. J. F. Enhancement Mechanisms of the Second Harmonic Generation from Double Resonant Aluminum Nanostructures. *ACS Photonics* **2017**, *4* (6), 1522−1530.
(12) Ding, S.; Yang, D.; Liu, X.; Nan, F.; Cheng, Z.; Im, S. J.; Zhou, L.; Wang, J.; Wang, Q. Asymmetric Growth of Au-Core/Ag-Shell Nanorods with a Strong Octupolar Plasmon Resonance and an Efficient Second-Harmonic Generation. *Nano Res.* **2018**, *11* (2), 686−695.
(13) Motl, N. E.; Smith, A. F.; Desantis, C. J.; Skrabalak, S. E. Engineering Plasmonic Metal Colloids through Composition and Structural Design. *Chem. Soc. Rev.* **2014**, *43* (11), 3823−3834.
(14) Jais, P. M.; Von Bilderling, C.; Bragas, A. V. Plasmon-Enhanced Second Harmonic Generation in Semiconductor Quantum Dots Close to Metal Nanoparticles. *Pap. Phys.* **2011**, *3* (0), 1−5.
(15) Linnenbank, H.; Grynko, Y.; Förstner, J.; Linden, S. Second Harmonic Generation Spectroscopy on Hybrid Plasmonic/Dielectric Nanoantennas. *Light: Sci. Appl.* **2016**, *5* (1), No. e16013.
(16) Singh, M. R. Enhancement of the Second-Harmonic Generation in a Quantum Dot-Metallic Nanoparticle Hybrid System. *Nanotechnology* **2013**, *24* (12), 125701.
(17) Shaviv, E.; Banin, U. Synergistic Effects on Second Harmonic Generation of Hybrid CdSe-Au Nanoparticles. *ACS Nano* **2010**, *4* (3), 1529−1538.
(18) Dorfs, D.; Härtling, T.; Miszta, K.; Bigall, N. C.; Kim, M. R.; Genovese, A.; Falqui, A.; Povia, M.; Manna, L. Reversible Tunability of the Near-Infrared Valence Band Plasmon Resonance in Cu2- XSe Nanocrystals. *J. Am. Chem. Soc.* **2011**, *133* (29), 11175−11180.
(19) Agrawal, A.; Cho, S. H.; Zandi, O.; Ghosh, S.; Johns, R. W.; Milliron, D. J. Localized Surface Plasmon Resonance in Semiconductor Nanocrystals. *Chem. Rev.* **2018**, *118* (6), 3121−3207.
(20) Xie, Y.; Carbone, L.; Nobile, C.; Grillo, V.; D'Agostino, S.; Della Sala, F.; Giannini, C.; Altamura, D.; Oelsner, C.; Kryschi, C.; et al. Metallic-like Stoichiometric Copper Sulfide Nanocrystals: Phase- and Shape-Selective Synthesis, near-Infrared Surface Plasmon Resonance Properties, and Their Modeling. *ACS Nano* **2013**, *7* (8), 7352−7369.
(21) Marin, B. C.; Hsu, S. W.; Chen, L.; Lo, A.; Zwissler, D. W.; Liu, Z.; Tao, A. R. Plasmon-Enhanced Two-Photon Absorption in Photoluminescent Semiconductor Nanocrystals. *ACS Photonics* **2016**, *3* (4), 526−531.
(22) Brzoska, J. B.; Shahidzadeh, N.; Rondelez, F. Evidence of a Transition Temperature for the Optimum Deposition of Grafted Monolayer Coatings. *Nature* **1992**, *360* (6406), 719−721.
(23) Goss, C. A.; Charych, D. H.; Majda, M. Applicaiton of (3-Mercaptopropyl)Trimethoxysilane as a Molecular Adhesive in the Fabrication of Vapor-Deposited Gold Electrodes on Glass Substrates. *Anal. Chem.* **1991**, *63* (1), 85−88.
(24) Motl, N. E.; Ewusi-Annan, E.; Sines, I. T.; Jensen, L.; Schaak, R. E. Experimental Determination of Composition and Correlation with Theory. *J. Phys. Chem. C* **2010**, *114*, 19263−19269.
(25) Metzger, B.; Hentschel, M.; Schumacher, T.; Lippitz, M.; Ye, X.; Murray, C. B.; Knabe, B.; Buse, K.; Giessen, H. Doubling the Efficiency of Third Harmonic Generation by Positioning ITO Nanocrystals into the Hot-Spot of Plasmonic Gap-Antennas. *Nano Lett.* **2014**, *14* (5), 2867−2872.
(26) Knittel, V.; Fischer, M. P.; De Roo, T.; Mecking, S.; Leitenstorfer, A.; Brida, D. Nonlinear Photoluminescence Spectrum of Single Gold Nanostructures. *ACS Nano* **2015**, *9* (1), 894−900.
(27) Wang, J.; Butet, J.; Baudrion, A. L.; Horrer, A.; Lévêque, G.; Martin, O. J. F.; Meixner, A. J.; Fleischer, M.; Adam, P. M.; Horneber, A.; et al. Direct Comparison of Second Harmonic Generation and Two-Photon Photoluminescence from Single Connected Gold Nanodimers. *J. Phys. Chem. C* **2016**, *120* (31), 17699−17710.
(28) Palomba, S.; Danckwerts, M.; Novotny, L. Nonlinear Plasmonics with Gold Nanoparticle Antennas. *J. Opt. A: Pure Appl. Opt.* **2009**, *11* (11), 114030.
(29) Ludwig, J.; An, L.; Pattengale, B.; Kong, Q.; Zhang, X.; Xi, P.; Huang, J. Ultrafast Hole Trapping and Relaxation Dynamics in p -Type CuS Nanodisks. *J. Phys. Chem. Lett.* **2015**, *6*, 2671.
(30) Davidson, R. B.; Ziegler, J. I.; Vargas, G.; Avanesyan, S. M.; Gong, Y.; Hess, W.; Haglund, R. F. Efficient Forward Second-Harmonic Generation from Planar Archimedean Nanospirals. *Nanophotonics* **2015**, *4* (1), 108−113.

https://dx.doi.org/10.1021/acsanm.0c00064
ACS Appl. Nano Mater. 2020, 3, 3144−3150